Supplementary information to "Dynamics of initiation, termination and reinitiation of DNA translocation by the motor protein EcoR124I"

Ralf Seidel, Joost G. P. Bloom, John van Noort, Christina F. Dutta, Nynke H. Dekker, Keith Firman, Mark D. Szczelkun, and Cees Dekker

Determination of the reinitiation time

We define a single translocation event as the time from when the DNA end-to-end distance starts to decrease due to translocation activity until the point where the end-to-end distance returns to its resting length due to termination of translocation.

Considering only one of the translocation directions of a bidirectionally translocating enzyme, the reinitiation time $T_{\text{reini},1} = T_{\text{bind,HsdR}} + T_{\text{ini}}$ is simply the time between the end of one translocation event and the start of new translocation event in that direction. The average measurement time to observe N_1 translocation events $\langle T_{\text{meas}} \rangle$ is then

$$\left\langle T_{\text{meas}} \right\rangle = \left\langle \sum_{\text{i}}^{\text{N1}} T_{\text{reini},1,\text{i}} + T_{\text{event},1,\text{i}} \right\rangle = N_1 \left(\left\langle T_{\text{reini},1} \right\rangle + \left\langle T_{\text{event},1} \right\rangle \right) \qquad \text{(S1)}$$

where $T_{\text{event},1,\text{i}}$ denotes the duration of the translocation event i in the specified direction. Let us now consider the second translocation direction, where within T_{meas} on average $\langle N_2 \rangle = \langle N_1 \rangle = \langle N_{\text{total}} \rangle/2$ events will be observed. Thus, using Eq. S1 the total number of events observed in average in the magnetic tweezers within T_{meas} results to

$$\left\langle N_{\text{total}} \right\rangle = \left\langle N_1 \right\rangle + \left\langle N_2 \right\rangle = \frac{T_{\text{meas}}}{\left\langle T_{\text{reini},1} \right\rangle + \left\langle T_{\text{event},1} \right\rangle} + \frac{T_{\text{meas}}}{\left\langle T_{\text{reini},2} \right\rangle + \left\langle T_{\text{event},2} \right\rangle} . \qquad \text{(S2)}$$

With $\langle T_{\text{reini},1} \rangle = \langle T_{\text{reini},2} \rangle = 2 \langle T_{\text{reini}} \rangle$ for the average reinitiation time between two translocation events in any direction and $\langle T_{\text{event},1} \rangle = \langle T_{\text{event},2} \rangle = \langle T_{\text{event}} \rangle$, one gets

$$\langle T_{\text{reini}} \rangle = \frac{T_{\text{meas}}}{\langle N_{\text{total}} \rangle} - \frac{\langle T_{\text{event}} \rangle}{2}. \qquad \text{(S3)}$$

For time traces consisting only of R_1-events $T_{\text{meas}} = \sum_{\text{i}} \left(T_{\text{between,i}} + T_{\text{event,i}} \right)$ with $T_{\text{between,i}}$ denoting the times between R_1-events (Fig. S1), which leads to

$$\langle T_{\text{reini}} \rangle = \frac{\sum_{\text{i}} \left(T_{\text{between,i}} + T_{\text{event,i}}/2 \right)}{N_{\text{total}}} = \frac{\sum_{\text{i}} T_{\text{reini,i}}}{N_{\text{total}}}. \qquad \text{(S4)}$$

This means that the individual reinitiation times $T_{\text{reini,i}}$ can, on average, be expressed by the sum of the time between two events $T_{\text{between,i}}$ and half of the event duration $T_{\text{event,i}}$ (Fig. S1). The same argument is true for R_2-events, although here one does not apply the whole event duration, but only the time between dissociation of the first and the second motor $T_{\text{R1,last}}$ (Suppl. Fig. 1). Note that N_{total} in Eq. S4 is corrected for R_1-events which remain undetected within the experimental noise (see below).

Equation S4 describes how $\langle T_{\text{reini}} \rangle$ is derived from the time traces. As it is important for the calculation of $k_{\text{bind,HsdR}}$ and k_{ini} (see main text), we add as a technical note that $\langle T_{\text{reini}} \rangle$ is the average time to reinitiate R_1-translocation activity after the end of a translocation event. It is therefore half the reinitiation times for translocation in only one direction ($\langle T_{\text{reini,1}} \rangle$,$\langle T_{\text{reini,2}} \rangle$). From this it follows that

$$\langle T_{\text{reini}} \rangle = \frac{1}{2} \langle T_{\text{reini,1}} \rangle = \frac{1}{2} \langle T_{\text{reini,2}} \rangle = \frac{1}{2} \left(\langle T_{\text{bind,HsdR}} \rangle + \langle T_{\text{ini}} \rangle \right). \qquad \text{(S5)}$$

Correction for undetected R_1-events

Whereas R_2-events generally result in translocation over long distances, R_1-events can be much shorter to the extent that they can even be in the range of the Brownian noise

fluctuations of the magnetic particle where they remain undetected. This is reflected in histograms of the event duration by a typical offset-time t_{off} (Suppl. Fig. 2). Events longer than t_{off} appear to follow an exponential distribution whereas the number of shorter events is much lower than expected from such a distribution. To obtain a correct total number of R_1-events $\langle N_{total} \rangle$, which goes into the calculations of $\langle T_{reini} \rangle$ and the R_2/R_1-ratio, the number of undetected events is estimated as follows.

We assume that the probability density $p(T_{event})$ for the event duration is distributed exponentially:

$$p(T_{event}) = \frac{1}{\langle T_{event} \rangle} \exp\left(-T_{event} / \langle T_{event} \rangle\right) \tag{S6}$$

Then the probability $P_{<toff}$ that an event will be shorter than t_{off} results to:

$$P_{<toff} = \int_0^{toff} p(T_{event}) dT_{event} = 1 - \exp\left(-t_{off} / \langle T_{event} \rangle\right). \tag{S7}$$

From this and from the number of events $N_{>toff}$ longer than t_{off} the number of events $N_{<toff}$ shorter than t_{off} can be estimated:

$$N_{<toff} = P_{<toff} \frac{N_{>toff}}{1 - P_{<toff}}. \tag{S8}$$

To estimate $N_{<toff}$ we obtain $\langle T_{event} \rangle$ from a maximum likelihood estimation of the event durations larger than t_{off} for Eq. S6, which is given by the analytical expression

$$\langle T_{event} \rangle = \frac{1}{N_{>toff}} \sum_i T_{event,i,>toff} - t_{off}. \tag{S9}$$

Fitting procedure for triplex displacement curves

To describe TFO displacement at different relative concentrations of DNA, MTase and HsdR, we used a kinetic scheme for triplex displacement (Suppl. Fig. 4), which is largely based on the scheme for reinitiation (Fig. 7). The practical implementation of this scheme relies on a lattice model for DNA translocation as previously described (McClelland et al., 2005; Firman and Szczelkun, 2000). The scheme takes into account that in forming the triplex, a fraction of productive HsdR binding events will not run towards a bound TFO (Suppl. Fig. 4A), but rather in the other direction. Under conditions where HsdR is in excess and every binding site is, on average, always occupied, we do not need to consider these alternative routes (e.g., see McClelland et al., 2005). However, where we are considering conditions where the HsdR-MTase association kinetics are limiting (e.g. Figures 2C and 4C in the main text) then we need to consider both routes as $HsdR_{free}$ may be artificially lowered by translocation events that cannot displace a triplex.

Triplex displacement curves were simulated and fitted to experimental data using numerical integration in Berkeley Madonna 8.0.1 (http://www.berkeleymadonna.com). The rate constant-dependent production and consumption of each species was represented as differential equations. The basic translocation scheme (Suppl. Fig. 4B) was altered for each spacing between triplex and EcoR124I site and solved by programming *n* differential equations for each step along the DNA. The concentration of MTase-DNA complexes was taken as the input concentration of DNA; this will be largely correct at the MTase concentrations used and over the time scales investigated. For initial values; M_{TFO} was set equal to c_{TFO}; M_{nil} was set equal to $2c_{DNA.MTase}$-M_{TFO}; HsdR was taken as c_{HsdR}. Dissociation events from the MTase-HsdR complex prior to initiation (from $M_{TFO}R_0$ and

$M_{nil}R_0$) were not considered. Simulations were used to obtain initial estimates of the values to be floated and subsequent fits were carried out using values both above and below the final values. One limitation of the fitting procedure, and one which was not considered in McClelland et al. (2005), is that the same profile is generated if the values for k_{ini} and k_{TFO} are switched. In other words, these two parameters cannot be determined independently.

Estimating the R_2/R_1-ratio and T_{lag} from the measured rate constants

With the magnetic tweezers we were able to measure the R_2/R_1-ratio and the lag time T_{lag} as a function of HsdR concentration (Fig. 6). Our derived reinitiation scheme (Fig. 7) should allow to derive these relations just from the measured rates in the reinitiation scheme, which is done in the following.

Given the slower HsdR binding rate for the stretched DNA molecules in the magnetic tweezers, R_2-activity will be mainly established starting from an already translocating R_1-complex (Fig. 7, red arrows), since HsdR binding at the experimental enzyme concentrations will be much slower than initiation of motor activity. Therefore R_2-event formation is governed by the competition between HsdR binding to the translocating R_1-complex ($k_{R2,2}$) and termination of R_1-translocation ($k_{off,R1}$). This yields a simplified relationship for the ratio between R_2 and R_1-events which is linearly dependent on HsdR concentration $R_2/R_1 \approx k_{R2,2}\, c_{HsdR}/k_{off,R1}$ (with $k_{R2,2} = k_{bind,HsdR} = 1.7 \times 10^6\ M^{-1}\ s^{-1}$ for stretched DNA). With this relation one obtains an HsdR concentration, at which an equal amount of R_2 and R_1-events occur, of about 230 nM, in reasonable agreement with the experimentally determined value of 150 nM (Fig. 6A). For the simplified model for R_2-

complex formation the lag-time can be approximated as $T_{lag} \approx (k_{R2,2}\ c_{HsdR} + k_{off,R1})^{-1}$, which closely describes the measured dependence of the lag time on the HsdR concentration (Fig. 6B).

Triplex displacement experiments with in vivo assembled EcoR124I

A central feature of our model (Fig. 7, main text) is that the HsdR subunits exchange on the core DNA-bound MTase. In the experiments presented here we have used endonuclease reconstituted *in vitro* from separately purified HsdR and MTase. It has been demonstrated previously for EcoR124I (Janscak et al, 1996; Janscak et al, 1998) and other Type I restriction enzymes (Dryden et al, 1997; Suri et al, 1984) that there is no difference in activity between *in vitro* reconstituted enzyme and directly purified *in vivo* assembled enzyme. However, it could be argued that whilst most activities are the same, the observed HsdR subunit exchange is specific to the *in vitro* reconstituted enzyme – that the endonuclease complex formed *in vivo* is more stable due to a slow protein-protein interaction step. To rule this possibility out, we examined whether the HsdR subunits on an *in vivo* assembled enzyme could readily exchange.

DNA triplex displacement experiments were carried out on 5 nM DNA using 1 nM *in vivo* assembled endonuclease (sample kindly provided by Pavel Janscak) with an average stoichiometry of two HsdR subunits per MTase as determined from SDS-PAGE gels according to Janscak et al (1998). Under these conditions, where the concentration of MTase is 1 nM and of HsdR ~2 nM, one should expect a maximum triplex displacement of ~20%. This is because the amount of triplex displacement should be limited by the amount of MTase, as the MTase has a long lifetime on the DNA compared to the

timescales used here (see main text). This is what was observed (Suppl. Fig. 5, lower profile). We then added additional MTase (50 nM) from the ATP syringe so that the free DNA sites would be saturated. If the HsdR subunits are tightly bound to the endonuclease complex, then they will not readily exchange onto the other MTases and the triplex displacement curves would be unaffected. However, if the HsdR subunits can readily exchange, then there should be both an increase in the total amplitude of displacement to 100% and an increase in the observed initial displacement rate. The results in Supp Fig. 5 (upper trace) clearly show a strong increase both in the initial rate and amplitude of the displacement. This can only be explained if the HsdR subunits from the endonuclease complex are exchanging between MTases. Therefore, the data as presented in the main section is not simply the result of our choice of enzyme reconstitution, but is equally relevant to *in vivo* assembled enzyme.

Characterization of the restriction alleviation deficient HsdR(A957V) mutant

To test whether the observed disassembly/assembly during EcoR124I translocation is relevant *in vivo* for the control of restriction alleviation (RA), we carried out experiments using an RA deficient mutant, HsdR(A957V). Makovets et al (2004) suggested that the increased cleavage efficiency of the EcoR124I RA^- mutants may be the result of increase complex stability. Alternatively, from the work presented here, one could also suggest that restriction activity can be controlled by the amount of available HsdR in the cell. To gain insight into the control mechanism, we present a preliminary characterization of HsdR(A957V) in terms of cleavage activity, triplex displacement and single-molecule

event frequencies. A more complete analysis of this and other RA mutants, along with details of the mutagenesis, will be presented elsewhere.

Cleavage was evaluated in the presence of ATP by incubating 5 nM supercoiled plasmid (pMDS27.13, 5.5 kbp) containing a single EcoR124I binding site with 30 nM MTase and increasing amounts of wildtype (wt) HsdR or HsdR(A957V). Strikingly, comparable levels of cleavage as measured by the disappearance of the supercoiled substrate and the production of linear product is observed for HsdR(A957V) at greatly reduced amounts of HsdR as compared to wtHsdR (Suppl. Fig. 6A,B). Full cleavage is obtained close to two HsdR(A957V) per plasmid (i.e. per DNA bound MTase or the stoichiometry of an R_2-complex). This is the most efficient cleavage ever reported for EcoR124I. For wtHsdR an ~8-fold excess of HsdR is required to get a comparable amount of cleavage in agreement with previous studies (Janscak et al, 1998).

Given that full cleavage activity with HsdR(A957V) is observed with ~2 HsdR per DNA bound MTase, one might speculate that the complex does not disassemble. To test this we carried out triplex displacement assays for substoichiometric amounts of HsdR to DNA bound MTase (5 nM HsdR, 5 nM DNA, 30 nM MTase). If complex disassembly were inhibited for HsdR(A957V), one should only expect ~50% triplex displacement. In contrast, we find full triplex displacement for HsdR(A957V) (Suppl. Fig 6C), which strongly suggests enzyme disassembly/reassembly. Furthermore, triplex displacement is faster than with wtHsdR. Additional experiments for concentrations of HsdR(A957V) as low as 0.5 nM (identical conditions as in Fig. 2C, see main text), where multiple HsdR turnovers are required for full triplex displacement, always exhibit full triplex displacement for HsdR(A957V) at higher rates than wtHsdR (data not shown).

Though the triplex displacement experiments strongly support that HsdR(A957V) undergoes dissociation/reassociation cycles, the faster triplex displacement could be either due to a higher cycling rate, for example as a result of faster binding, or due to a more efficient triplex displacement, for example as a result of a higher processivity. To investigate these alternatives we measured translocation activity at 10 nM HsdR(A957V) in the magnetic tweezers. Plotting the cumulative number of translocation events versus time (Suppl. Fig. 6D), we find a strongly increased number of events, close to the activity seen at 6-fold higher concentration of wtHsdR (Fig. 2, main text). In addition, the number of R_2-events matches that seen at a much higher wtHsdR concentration (Suppl. Fig. 6D, filled circles). We have yet to observe any significant improvement in the processivity of R_1 or R_2-events for HsdR(A957V) compared to wtHsdR (data not shown). This suggests that the increased activity of HsdR(A957V) in the cleavage and translocation assays is due to faster HsdR binding/initiation of translocation.

In conclusion, using three different assays we find a significantly increased activity of HsdR(A957V) compared to wt HsdR. Comparable levels of activity are observed for wtHsdR at a ~4-fold higher concentration. Although one could argue that the fraction of active HsdR(A957V) in the given enzyme preparation is greater, we note to the best of our knowledge that all preparations of wtEcoR124I or wtHsdR (including our own), carried out in different laboratories, always required a ~8-fold excess of enzyme over EcoR124I binding sites (Janscak et al, 1996; Bianco & Hurley, 2005; Janscak et al, 1998; Szczelkun et al, 1997). To gain independent evidence for relative activity of HsdR(A957V), we carried out gel shift experiments to reveal the assembly state of the enzyme complex (R_1, R_2-complex), which is dependent on the concentration of HsdR in

the sample (Janscak et al, 1998). The band shift experiments (data not shown) showed that comparable levels of R_1 and R_2-complexes are reached at the same concentrations of either wtHsdR or mutant HsdR. This would not be the case if the fraction of active mutant HsdR in the sample were significantly different from the wtHsdR preparation. We are therefore very confident that the increased activity of HsdR(A957V) in the three applied assays is an intrinsic property of the mutant. Moreover, since this mutant shows an elevated level of motor events and cleaves DNA more efficiently, both *in vitro* and *in vivo*, we are confident that the model presented in Figure 7, where the amount of HsdR dictates the number and frequency of motors events, will play a crucial role in RA in the cell.

The observation that for the RA deficient HsdR(A957V) the general reinitiation scheme for translocation, via rebinding of HsdR, remains unchanged with the exception that similar levels of activity are reached at reduced HsdR concentrations, strongly suggest that RA is controlled by the amount of free HsdR in the cell. This implies that within the cell the expression of HsdR is kept at a level, at which R_2-complexes and thus cleavage rarely occur. Indeed for EcoKI, analysis of cell extracts reveals that HsdR is much less abundant than the MTase subunits HsdS and HsdM (Weiserova et al, 1993). For HsdR(A957V) the threshold to establish translocation, in particular R_2-events, is significantly lowered, which we could directly relate to an increased rate of cleavage (compare Suppl.Figs. 6A,B and 6D). This in turn increases the probability that an unmethylated EcoR124I binding site is used to cleave the chromosomal DNA, potentially inhibiting RA.

Our model, which proposes that HsdR expression is kept at a level, at which cleavage is prevented, is somewhat similar to Type IA and IB restriction enzymes. For those systems the protease ClpXP prevents the formation of translocating complexes (Makovets et al, 1999). We note that the mechanism of restriction alleviation, in particular for EcoR124I, still deserves further research. From our first characterization of an RA deficient mutant, however, we are able to propose a testable model for the control of RA by EcoR124I. Additional *in vivo* experiments, for example by varying the expression levels of HsdR, should directly prove our model.

References

Bianco PR, Hurley EM (2005) The type I restriction endonuclease EcoR124I, couples ATP hydrolysis to bidirectional DNA translocation. *J Mol Biol* in press

Dryden DTF, Cooper LP, Thorpe PH, Byron O (1997) The in vitro assembly of the EcoKI type I DNA restriction/modification enzyme and its in vivo implications. *Biochemistry* **36:** 1065-1076

Janscak P, Abadjieva A, Firman K (1996) The type I restriction endonuclease R.EcoR1241: Over-production and biochemical properties. *J Mol Biol* **257:** 977-991

Janscak P, Dryden DTF, Firman K (1998) Analysis of the subunit assembly of the type IC restriction-modification enzyme EcoR124I. *Nucleic Acids Res* **26:** 4439-4445

Makovets S, Doronina VA, Murray NE (1999) Regulation of endonuclease activity by proteolysis prevents breakage of unmodified bacterial chromosomes by type I restriction enzymes. *Proc Natl Acad Sci U S A* **96 :** 9757-9762

Makovets S, Powell LM, Titheradge AJB, Blakely GW, Murray NE (2004) Is modification sufficient to protect a bacterial chromosome from a resident restriction endonuclease? *Mol Microbiol* **51:** 135-147

McClelland SE, Dryden DTF, Szczelkun MD (2005) Continuous assays for DNA translocation using fluorescent triplex dissociation: application to type I restriction endonucleases. *J Mol Biol* **348:** 895-915

Seidel R, van Noort J, van Der Scheer C, Bloom JGP, Dekker NH, Dutta CF, Blundell A, Robinson T, Firman K, Dekker C (2004) Real-time observation of DNA translocation by the type I restriction modification enzyme EcoR124I. *Nat Struct Mol Biol* **11:** 838-843

Suri B, Shepherd JCW, Bickle TA (1984) The EcoA restriction and modification system of Escherichia coli 15T: Enzyme structure and DNA recognition sequence. *EMBO J* **3:** 575-579

Szczelkun MD, Janscak P, Firman K, Halford SE (1997) Selection of non-specific DNA cleavage sites by the type IC restriction endonuclease EcoR124I. *J Mol Biol* **271:** 112-123

Weiserova M, Janscak P, Benada O, Hubacek J, Zinkevich VE, Glover SW, Firman K (1993) Cloning, production and characterization of wild-type and mutant forms of the REcoK endonuclease. *Nucleic Acids Res* **21:** 1686

Supplementary Figures

Suppl. Fig 1: Determination of the mean time to reinitiate translocation $\langle T_{reini} \rangle$. The time to reinitiate translocation of the first motor subunit after disassembly of the complex is, on average, the time between two translocation events $T_{between}$ plus half of the event time T_{event} for an R_1-event or half of the translocation time of the second dissociating motor $T_{R1,last}$ for an R_2-event. Averaging over all the individual reinitiation times $T_{reini,i}$ provides $\langle T_{reini} \rangle$. We need to consider the translocation times as part of T_{reini} due to the fact that a R_1-complex can already bind a second HsdR while it is still translocating.

Suppl. Fig. 2: Estimating undetected R_1-events. A) Histograms of the duration of R_1-events (T_{event}) recorded at 0.8 pN. The black line is the maximum likelihood estimate (Eq. S9) for the events longer than t_{off} = 0.5 s assuming an exponential distribution (Eq. S6). From the fit a mean event duration of 1.5 s is obtained. The number of events shorter than 0.5 s is significantly underestimated because the corresponding translocation distances are within the range of the Brownian noise fluctuations of the magnetic bead. B) The number of R_1-events shorter than t_{off} is estimated using the exponential distribution obtained in A and Eq. S8.

Suppl. Fig. 3: Triplex displacement profiles for different MTase concentrations. The final MTase concentrations are indicated. Reactions were initiated by mixing preincubated triplex DNA, MTase and HsdR with an equal volume of reaction buffer with ATP (final concentration 4 mM). The triplex is 2047 bp away from the EcoR124I binding site. The

final HsdR concentration is 4 nM and the DNA concentration is 5 nM, of which 2.5 nM carry the triplex. The triplex displacement profiles are unaffected by the MTase concentration. Therefore, association of free HsdR with free MTase is a very unlikely event. Otherwise a strong decrease in the triplex displacement rate should be observed for increasing MTase concentrations, because association between HsdR and MTase would reduce the free HsdR concentration and thus slow down resetting, which dominates the kinetics under the reaction conditions described here.

Suppl. Fig. 4: Kinetic scheme for triplex displacement. A) Fate of HsdR binding events in the triplex assay. The TFO binding site is on one side of the Type I site only. Triplex DNA is formed using a substoichiometric amount of TFO. A sufficient molar excess of MTase is added such that the Type I recognition sites are saturated. Each MTase has two motor binding sites and the HsdR subunits associate with the MTase independently. Because of the nature of the Triplex substrates, there are two fates of an HsdR binding event: 1) binding to M_{TFO}, where translocation by the HsdR subunit can either result in triplex displacement or dissociation from the DNA; or, 2) binding to M_{nil}, where translocation by the HsdR subunit cannot result in triplex displacement and only dissociation from the DNA can occur. All kinetic parameters for the M_{TFO} and M_{nil} sites are identical. As the reaction progresses and triplex is displaced, the pool of M_{nil} sites will increase. B) Kinetic scheme based on Figure 7 and taking into account the considerations of the triplex assay (see text). The M_{TFO} and M_{nil} sites are considered independently. The model assumes that following triplex displacement translocation can continue. Translocation from either M_{TFO} or M_{nil} sites can result in an HsdR subunit entering an

"*infinite" translocation pool*; this assumes that the DNA is infinitely long and therefore dissociation from DNA ends is not considered. Translocation to a DNA end is a low probability event with the DNA substrates used here.

Suppl. Fig. 5: Triplex displacement profiles for purified *in vivo* assembled enzyme (R.EcoR124I) with and without additional MTase. Reactions were initiated by mixing preincubated triplex DNA and R.EcoR124I with an equal volume of reaction buffer with ATP (final concentration 4mM) and, where indicated, MTase (final concentration 50 nM). The final DNA concentration is 5 nM.. The triplex is 2047 bp away from the EcoR124I site. The triplex displacement profiles (black lines) were fitted by a single exponential $P(t) = P_{Max}(1-\exp(-k\,t))+P_0$ (red lines). This provided a maximum fraction of displaced triplex $P_{Max,no\ MTase} = 0.21 \pm 0.01$ or $21 \pm 1\%$, a reaction rate $k_{no\ MTase} = 2.8 \pm 0.1 \times 10^{-3}\ s^{-1}$, and an initial displacement velocity $V_{no\ MTase} = P_{Max,no\ MTase}\ k_{no\ MTase} = 0.59 \pm 0.05 \times 10^{-3}\ s^{-1}$ in the absence of additional MTase. In the presence of additional MTase $P_{Max,with\ MTase} = 0.94 \pm 0.01$ or $94 \pm 1\%$, $k_{with\ MTase} = 2.2 \pm 0.1 \times 10^{-3}\ s^{-1}$, and $V_{with\ MTase} = 2.1 \pm 0.1 \times 10^{-3}\ s^{-1}$ were obtained.

Suppl. Fig. 6: Characterization of the restriction alleviation deficient HsdR(A957V) mutant. A) Agarose gel assays to monitor cleavage for increasing amounts of HsdR carried out for wildtype (wt) HsdR and HsdR(A957V). 5 nM of ^{3}H-labelled pMDS27.13 (containing a single EcoR124I binding site) was incubated for 1 hour in buffer R supplemented with 30 nM MTase, wtHsdR and HsdR(A957V) as indicated in the figure and 4 mM ATP. Reaction products were separated in a 1% (w/v) agarose gel containing

ethidium bromide. ccc denotes the supercoiled covalently closed circular DNA template, oc the nicked open circular and lin the linearized reaction products. B) Amount of substrate ccc plasmid for increasing amounts of HsdR from the experiments in A. The DNA was quantified by scintillation counting C) Triplex displacement profiles for wtHsdR and HsdR(A957V). Reactions were initiated by mixing preincubated triplex DNA, HsdR and MTase with an equal volume of reaction buffer with ATP. The final solution contains 5 nM DNA, 5 nM HsdR, 30 nM MTase and 4 mM ATP. The triplex is 6888 bp away from the EcoR124I binding site. The inset is a zoom into the triplex displacement curves showing the initial 45 s of the reaction. D) Cumulative event number versus time for 10 nM HsdR(A957V) obtained from magnetic tweezers measurements (black circles). The MTase concentration is 20 nM and the applied stretching force 1.7 pN. Open circles indicate R_1-events, filled circles R_2-events. Data for different concentrations of wtHsdR (gray circles) was taken from Fig. 2B (see main text).

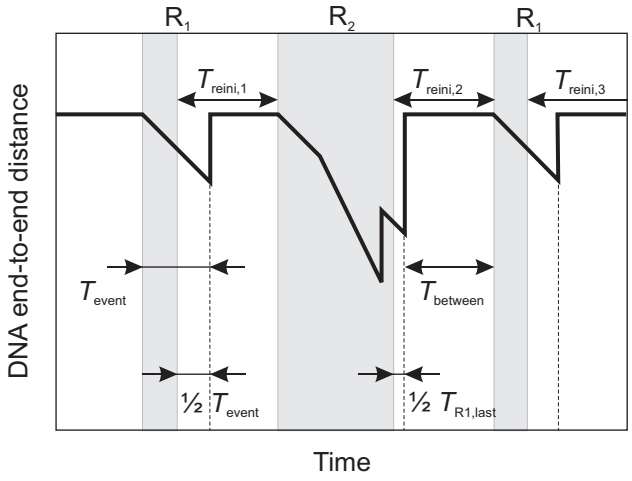

Supplementary figure 1

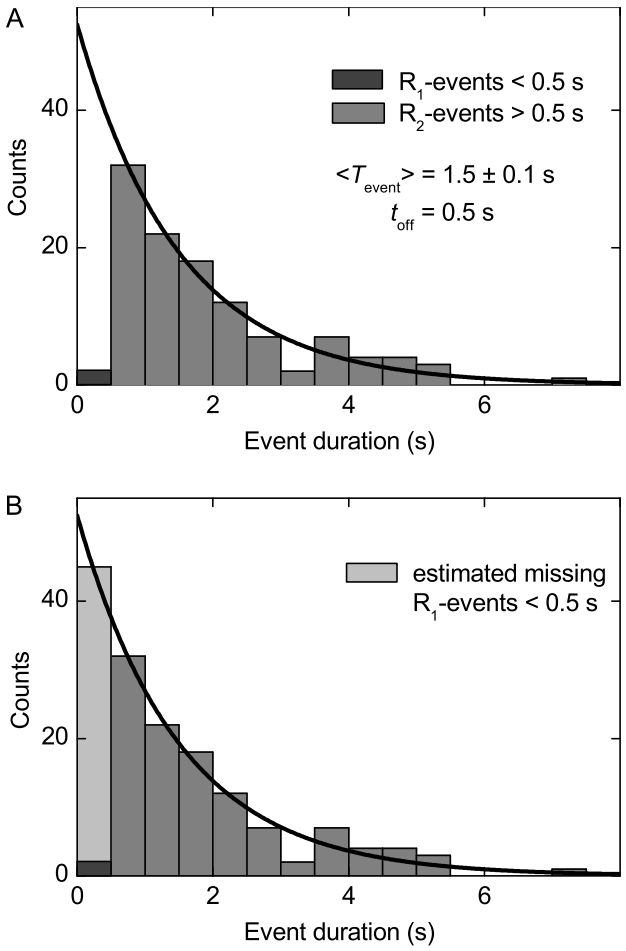

Supplementary figure 2

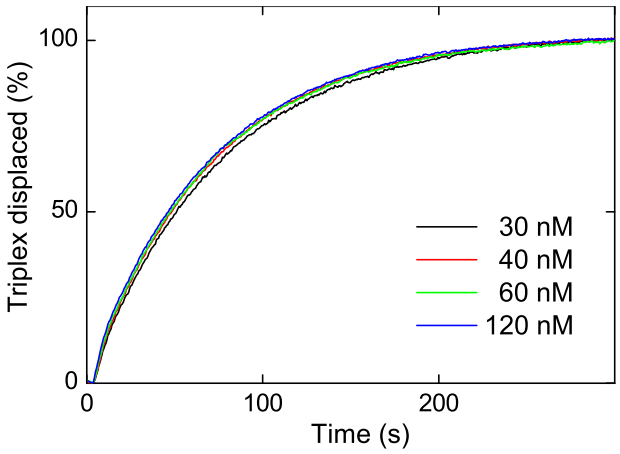

Supplementary figure 3

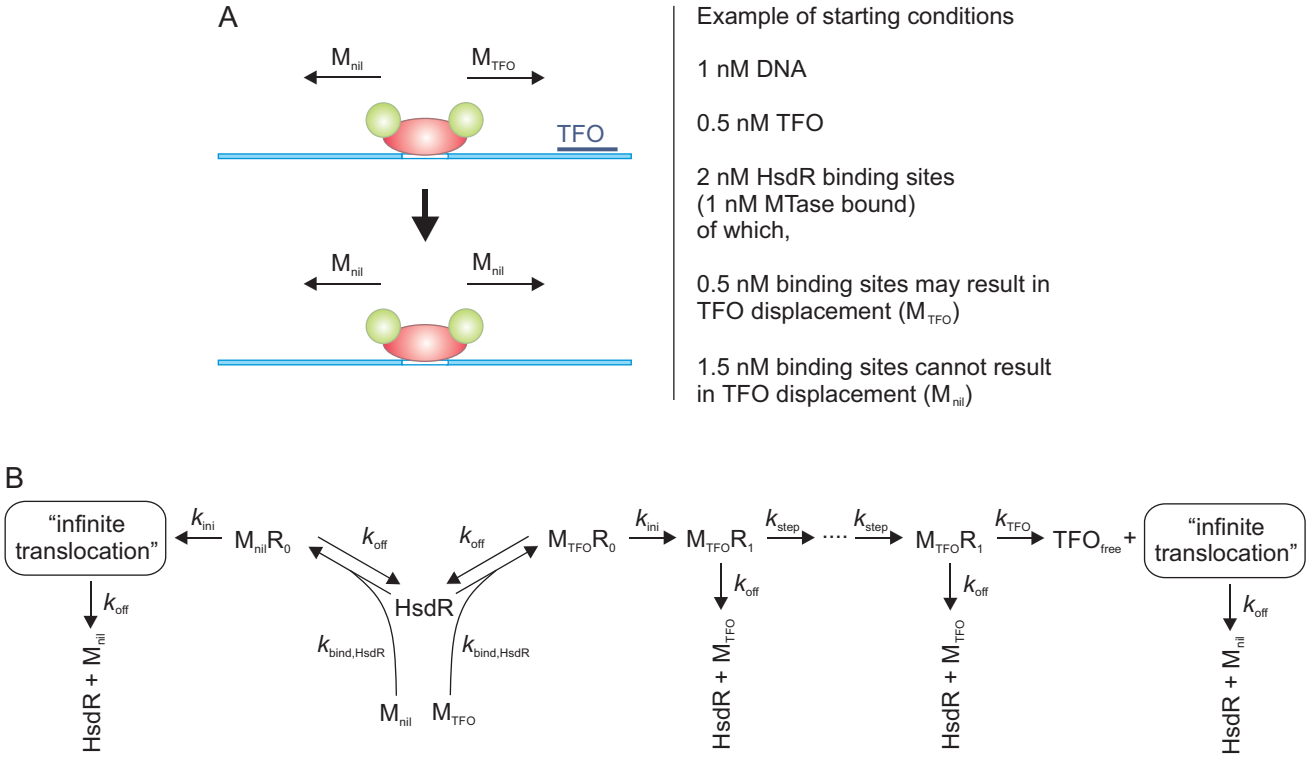

Supplementary figure 4

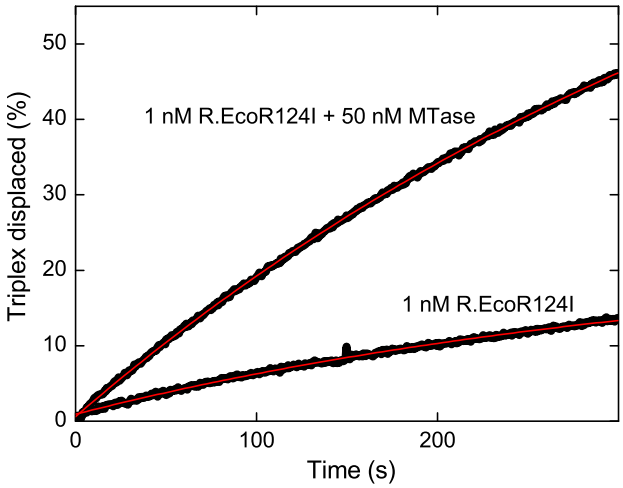

Supplementary figure 5

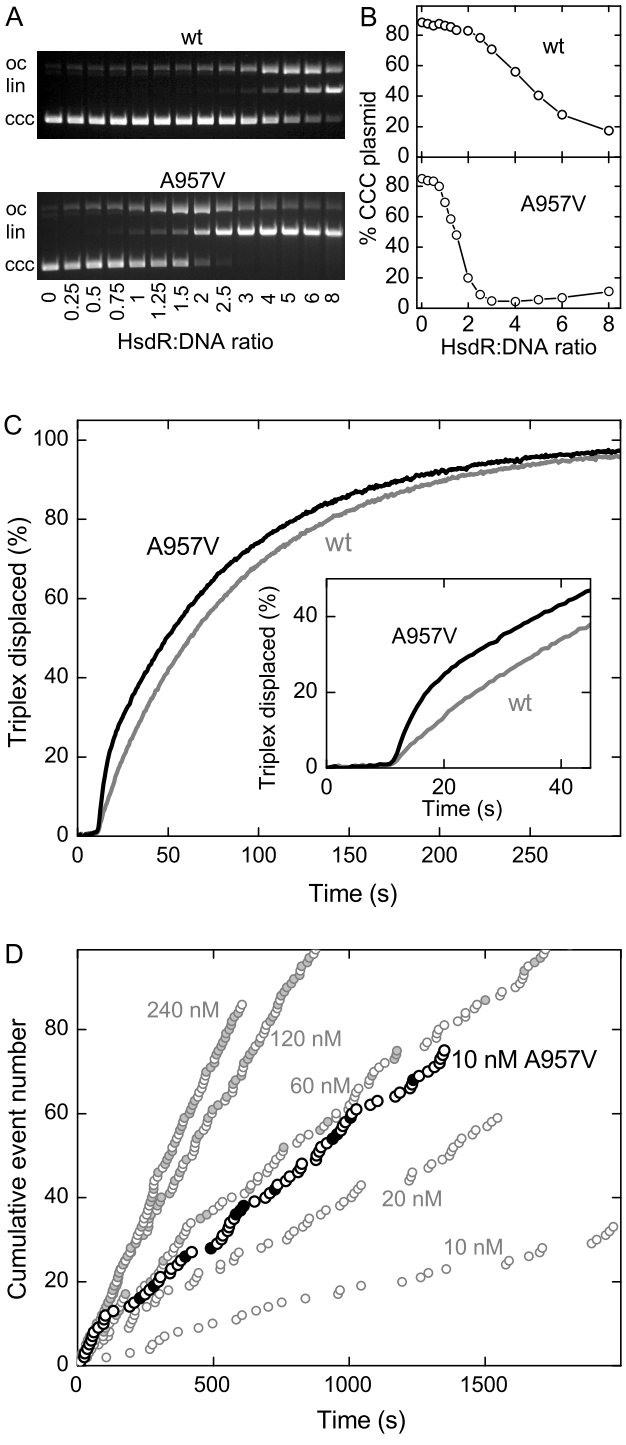

Supplementary figure 6